Multi-wavelength search for quasi-periodic oscillations in BL Lac 4FGL J0112.1+2245

Y.L. Gong[1,2] · T.F. Yi[1,2] [ID] · X. Yang[3,2] · H.Z. Li[4] · X. Chang[1] · J.P. Chen[1] · Z.H. Chen[1]

Abstract

We have assembled historical light curve data of the BL Lac object 4FGL J0112.1+2245 at radio, optical and γ-ray bands, spanning about a 12.5, 8.4, and 11.9 yr period, respectively. We used the Lomb-Scargle Periodogram (LSP), Weighted Wavelet Z-transform (WWZ) and epoch folding methods to search for periodicity in the light curves. The results indicate that there is a possible quasi-periodic oscillation (QPO) of 896 ± 32 days for γ-rays, 880 ± 54 days in the optical, and 830 ± 33 days in the radio band, respectively. In addition, the QPO signals evaluated by employing a red noise model were found to be above 3 σ (99.7%) in the three bands. Assuming that it originates from a jet in helical motion in a supermassive binary black hole system undergoing a merger, we estimate the primary black hole mass $M \simeq 2.2 \times 10^9 M_\odot$. Using the discrete correlation function (DCF) method, we investigated the correlation among multi-wavelength bands, and found that there is a significant correlation between the different bands from MJD 57670 to 59000. The results indicated that the optical flux in this source is originating from the same or vicinal emission region as the γ-ray and show a time lag of 73 days with radio band. Across the data as a whole, the DCF results show that the optical correlation with radio and γ-ray is significant, while the correlation between the γ-ray and radio bands are weak.

1 Introduction

Blazars are a subtype of active galactic nuclei (AGN) with relativistic jet pointing towards the Earth (Urry and Padovani 1995). The features of the blazars are rapid and violent variability at all wavelengths, and a high degree of linear polarization in the optical band and non-thermal continuum emission ranging from radio to high-energy γ-rays (Angel and Stockman 1980; Xiong et al. 2017). Accord-

ing to the features of the optical emission lines, blazars are usually divided into two sub-class: BL Lacertae objects (BL Lacs) and flat-spectrum radio quasars (FSRQs). BL Lacs show weak or no emission lines, and FSRQs show strong emission lines. BL Lacs are further classified as low-frequency peaked BL Lacs (LBLs), intermediate-frequency peaked BL Lacs (IBLs) and high-frequency peaked BL Lacs (HBLs) based on the peak frequency of their synchrotron component, ν_{peak}: for LBLs $\log \nu_{peak} < 14$, for IBLs $14 < \log \nu_{peak} < 15$, and for HBLs $\log \nu_{peak} > 15$ (Shaw et al. 2013).

Research on quasi-periodic oscillations (QPOs) of blazars is one of the most active fields of extragalactic astronomy and provides an important way to explore the radiation process in blazars (Li et al. 2018). However, the QPOs in blazars are rare and transient (Zhou et al. 2018; Gupta et al. 2019). At present, the periodicity of multi-wavelengths variabilities of many sources has been explored by many researchers, e.g., 3FGL J0449.4-4350 (Yang et al. 2020), MrK 421 (Gaur et al. 2012; Li et al. 2016), PG 1553+113 (Ackermann et al. 2015; Sobacchi et al. 2017; Yan et al. 2018). And Peñil et al. (2020) systematically searched for periodical variability of

✉ T.F. Yi
yitingfeng98@163.com

H.Z. Li
lhz@yxnu.net

1   Physics Department, Yunan Normal University, Kunming, Yunnan, 650092, China

2   Guangxi Key Laboratory for the Relativistic Astrophysics, Nanning 530004, China

3   GXU-NAOC Center for Astrophysics and Space Sciences, Department of Physics, Guangxi University, Nanning 530004, China

4   Physics Department, Yuxi Normal University, Yuxi 53100, China

γ-rays band of blazars. Astronomers have discovered a supermassive black hole (SMBH) lurking in the center of most galaxies (Cavaliere and Padovani 1989; Chokshi and Turner 1992). The SMBH binary system has been widely invoked to explain some blazar observational phenomena (Graham et al. 2015a,b; Charisi et al. 2016; Zhang et al. 2020). The mechanism leading to the QPO of blazars is still an open question.

Blazars emit over the entire accessible electromagnetic spectrum. Studying the correlation between different wavelengths can provide useful constraints for the model of the blazars structure and emission process. Many researchers have studied the correlation between the different waveband's variability of some sources, e.g., OJ 287 (Valtaoja et al. 1987), 3C 273 (Valtaoja et al. 1991; Robson et al. 1993; Dai et al. 2006). Blazar 4FGL J0112.1+2245 (RA = 01h 12m 5.8s, Dec = +22d 44m 38.8s; GC 0109+224, S2 0109+22) is a TeV BL Lac object (log ν_{peak} = 14.325, IBL), with redshift $z = 0.265$ and has a doppler factor $\delta = 8.5$ (Wu et al. 2007, 2009). Ciprini et al. (2004) used the z-transformed discrete correlation function (ZDCF) to study the correlation between optical and radio (8 GHz, 14.5 GHz, 22 GHz, 37 GHz) for this source (4FGL J0112.1+2245). They found only one weak correlation between the optical and radio bands (ZDCF coefficient $\simeq$ 0.5–0.6 and time lag $\simeq$ 900 days). MAGIC Collaboration et al. (2018) also investigated the correlation between optical R and 15 GHz radio bands of this source using discrete correlation function (DCF) methods. They calculated that a DCF peak value significance ($< 2\sigma$) suggested that there was no correlation between the two bands. Is there really no correlation between the optical and radio bands of this source?

In this paper, to search QPO and the correlation between the different bands, we assembled the historical light curve data of 4FGL J0112.1+2245 at radio from Owens Valley Radio Observatory (OVRO), optical from Katzman Automatic Imaging Telescope (KAIT), and γ-ray band from Fermi-LAT data center. This source shows drastic changes in all three bands, especially in 2018 there is a very obvious big flare. We used three methods to analyze the long-term observations data of BL Lac 4FGL J0112.1+2245 and report our discovery of a high confidence QPO of the three bands flux variability. In Sect. 2, we briefly describe the data collection and reduction. In Sect. 3, we present the three methods of searching for the QPO of the BL Lac. In Sect. 4, we present a correlation analysis between the three bands. In Sect. 5, we provide a discussion and conclusions.

2 Data reduction

We presented the variability data of J0112.1+2245 at radio 15 GHz, optical, 0.1–300 GeV γ-ray (bin = 30 days) and 0.1–300 GeV γ-ray (bin = 7 days). We use fractional variability to characterize the variability of different bands, the formula is defined as (Vaughan et al. 2003; Aleksić et al. 2015; Ren et al. 2021):

$$F_{var} = \sqrt{\frac{S^2 - \langle \sigma_{err}^2 \rangle}{\langle x \rangle^2}}, \tag{1}$$

where S represents the standard deviation of the flux, $\langle \sigma_{err}^2 \rangle$ represents the mean square error and $\langle x \rangle^2$ represents the square of the average flux. At the same time, we also evaluated the uncertainty of F_{var}. The expression is as follows (Aleksić et al. 2015):

$$\triangle F_{var} = \sqrt{F_{var}^2 + err(\sigma_N^2)} - F_{var}, \tag{2}$$

however, $err(\sigma_N^2)$ is obtained by Vaughan et al. (2003):

$$err(\sigma_N^2) = \sqrt{\left(\sqrt{\frac{2}{N}}\frac{\langle \sigma_{err}^2 \rangle}{\langle x \rangle^2}\right)^2 + \left(\sqrt{\frac{\langle \sigma_{err}^2 \rangle}{N}}\frac{2F_{var}}{\langle x \rangle}\right)^2}, \tag{3}$$

here, N is the number of data points set. From the above formula, we get $F_{var} = 0.71 \pm 0.02$, 0.59 ± 0.02, 0.44 ± 0.004 and 0.44 ± 0.002 for γ-ray (bin = 7 days), γ-ray (bin = 30 days), optical, and radio bands, respectively. These results show that there is great variability in γ-ray band, while the variability is moderate in optical and radio bands.

2.1 Radio and optical data

The 15 GHz radio data of 4FGL J0112.1+2245 were taken from the 40 m telescope at the Owens Valley Radio Observatory (OVRO).[1] The number of data points is 779. The light curve of 15 GHz spans about 12.5 yr from 2008 January 7 to 2020 July 1. In the radio band, in addition to the large flare in 2009 and 2018, there are many flares with different amplitudes.

The optical R band data of 4FGL J0112.1+2245 were taken from the 0.76 m Katzman Automatic Imaging Telescope (KAIT). The KAIT monitored a light curve of a total of 163 AGNs with an average rhythm of 3 days. The effective color is similar to R-band. The number of data points is 272 (MJD 55807 to 58859). The quasi-periodic oscillation (QPO) and discrete correlation function (DCF) are analyzed by converting R-band data from magnitude to absolute flux density (Bessell 1979).

2.2 Gamma-ray data

The public γ-ray data of 4FGL J0112.1+2245 are obtained from the observations of the Large Area Telescope (LAT)

---

[1]https://sites.astro.caltech.edu/ovroblazars.

Fig. 1 Light curves of 4FGL J0112.1+2245 in the 15 GHz radio, optical R, 0.1–300 GeV γ-ray in 30 days bin, and 0.1–300 GeV γ-ray bands in 7 days bin. The red dash-dotted line indicates a similar flare in the three bands. The blue dashed line indicates MJD = 57670 position
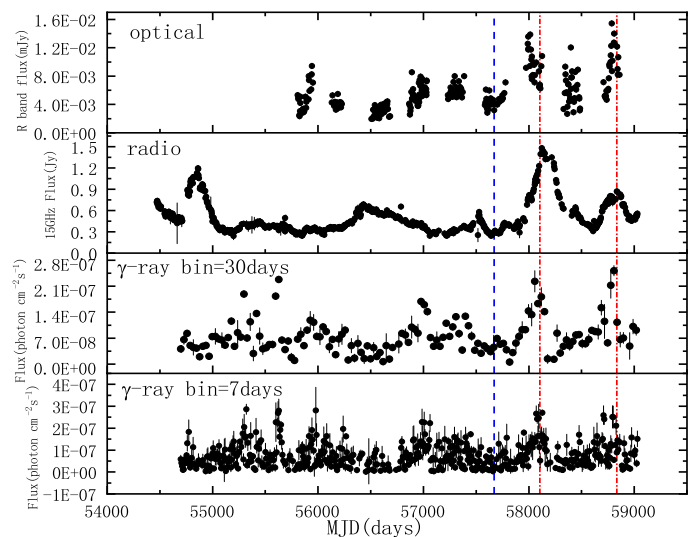
(Abdo et al. 2009; Atwood et al. 2009). The LAT data analysis employs the Fermi Science Tools version v11r06p03 package. We used the "P8R3_SOURCE_V2" instrument response functions and selected "SOURCE" class events in the 0.1–300 GeV energy range from a 10° radius region of interest (ROI) centered on the source location with 105° as the zenith cut. The diffuse γ-rays emission of the galactic and extragalactic are modeled using two files: gll_iem_v07.fit and iso_P8R3_SOURCE_V2_v1.txt. We use the script make4FGLxml.py to generate the model file. The XML model used in the fit includes sources within ROI +10°, so the fits account for contributions from sources outside the ROI. Using this procedure, we generate 7 days and 30 days binned γ-ray light curves. The period chosen for the analysis covers a mission elapsed time range of 239,557,418 to 616,769,496 s, or 2008 August 4 15:43:37 to 2020 July 18 12:51:31 UTC. Finally, a likelihood ratio test statistic (TS = $2 \log L_1 - 2 \log L_0$) was performed to estimate the significance of the γ-rays events from the source (Abdo et al. 2010; Bhatta 2017). The photon flux light curve of the source is the result of cutting with TS > 10 (equivalent to a > 3.2σ detection; $\sqrt{TS}\sigma$; Mattox et al. (1996)). The following analysis of light curves is based on this new model file.

3 Methods for periodicity search and analysis results

Lomb-Scargle Periodogram (LSP) is a method widely used in searching for quasi-periodic oscillations (Lomb 1976; Scargle 1982; Press et al. 1992). For the non-uniform sampling time series $x(t_i)$, $i = 1, 2, 3 \cdots, N$, the power spec-

trum is defined as:

$$P_{LS}(f) = \frac{1}{2N} \times \left[\frac{\left\{ \sum_{i=1}^{N} x(t_i) \cos\left[2\pi f(t_i - \tau)\right] \right\}^2}{\sum_{i=1}^{N} \cos^2\left[2\pi f(t_i - \tau)\right]} \right.$$

$$\left. + \frac{\left\{ \sum_{i=1}^{N} x(t_i) \sin\left[2\pi f(t_i - \tau)\right] \right\}^2}{\sum_{i=1}^{N} \sin^2\left[2\pi f(t_i - \tau)\right]} \right]^2, \quad (4)$$

where f and τ represent the test and the time offset, respectively, which can be obtained by the relation:

$$\tan(2\pi f\tau) = \frac{\sum_{i=1}^{N} \sin 2\pi f t_i}{\sum_{i=1}^{N} \cos 2\pi f t_i}. \quad (5)$$

We assessed the confidence level of our findings by modeling the multi-wavelength variability as red noise with a power law index β. To estimate the confidence level based on the power law red noise model, 10,000 light curves were simulated by the method described in Timmer and Koenig (1995) for each of the power law index β values. For obtaining the β index of each wavelength band, we fitted the spectrum of the periodogram with a power law, $p(f) \propto f^{-\beta}$ (for details see our previous paper (Yang et al. 2020)). The β index value is shown in Table 1. Once the 10,000 light curves were simulated by using even sampling intervals, and their LSP was computed. Consequently, using the spectral distribution of the simulated light curves, local 95%, 99%, 99.7% (3σ) and 99.99% (4σ) confidence contour lines were evaluated. As shown in the right panels of Figs. 2, 3, there are two obvious peaks in the periodogram, which hint two possible QPOs with 900 ± 34 and 344 ± 13 days for 0.1–300 GeV γ-ray (bin = 30 days) band. For 0.1–300 GeV γ-ray (bin = 7 days) band, there are two peaks in the periodogram, which
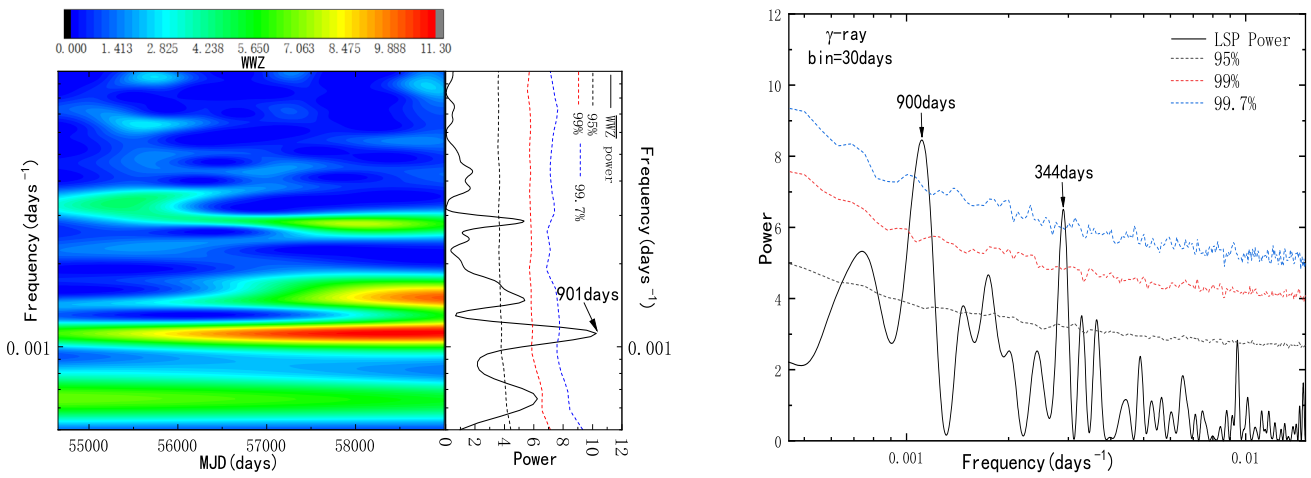
Fig. 2 Left panel: 2D plane contour plot of the WWZ power of the γ-ray band (0.1–300 GeV) with 30 days bin light curve. The black solid line represents the time-averaged WWZ power. Right panel: cor-responding LSP power spectrum (black solid line); The black, red, and blue dashed lines represent the confidence level of 95%, 99%, and 99.7% respectively
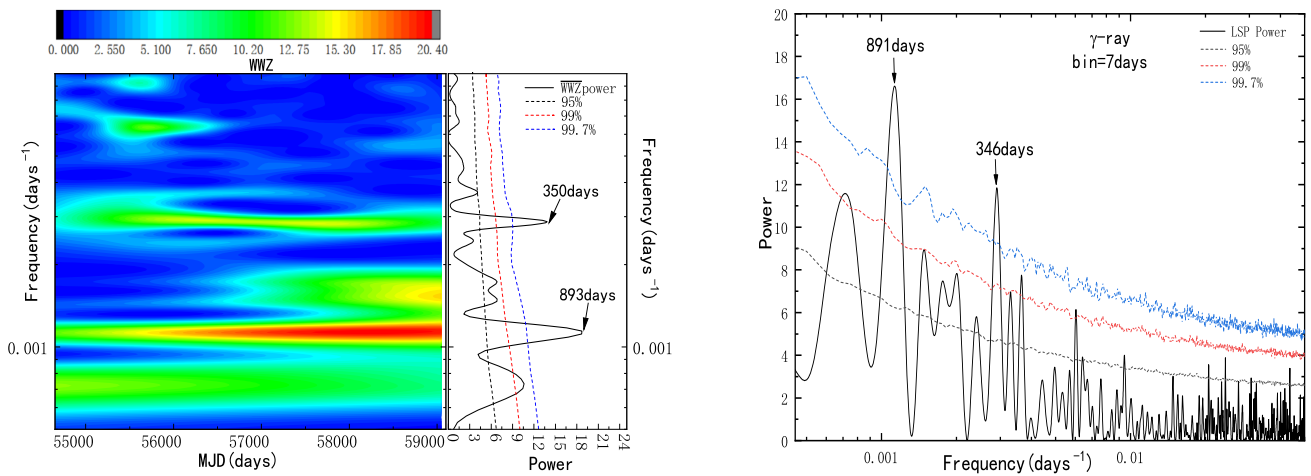
Fig. 3 Same as Fig. 2, but with the 7-days bin

Table 1 Summary of the results of the periodicity analysis in multi-wavelength bands for 4FGL J0112.1+2245

| Bands	γ-ray 30 days bin	Conf.[b]	γ-ray 7 days bin	Conf.[b]	Optical R band	Conf.[b]	Radio 15 GHz	Conf.[b]
LSP (days)	900 ± 34	>99.7%	891 ± 25	>99.7%	877 ± 57	≈99.99%	827 ± 35	≈99.99%
	344 ± 13	>99.7%	346 ± 11	>99.7%				
WWZ (days)	901 ± 39	>99.7%	893 ± 31	>99.7%	884 ± 51	≈99.99%	833 ± 32	>99.7%
			350 ± 15	>99.7%				
β[a]	0.6		0.5		0.7		1.1	

Notes:

[a]The power law index

[b]The confidence level of periodic signal

possible QPOs of 891 ± 25 and 346 ± 11 days. In Fig. 4, for the optical R band, there is one obvious peak in the peri-odogram, which possible QPO of 877 ± 57 days. In Fig. 5, for the 15 GHz radio band, there is one obvious peak in the
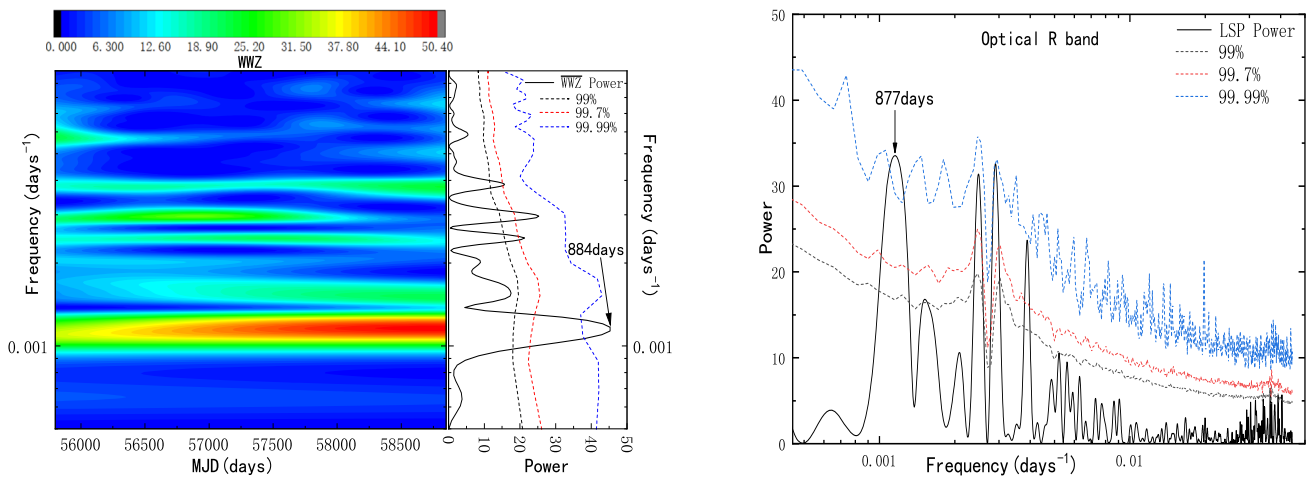
Fig. 4 Left panel: 2D plane contour plot of the WWZ power of the optical R band light curve. The black solid line represents the time-averaged WWZ power. Right panel: corresponding LSP power spectrum (black solid line); The black, red, and blue dashed lines represent the confidence level of 99%, 99.7%, and 99.99% respectively
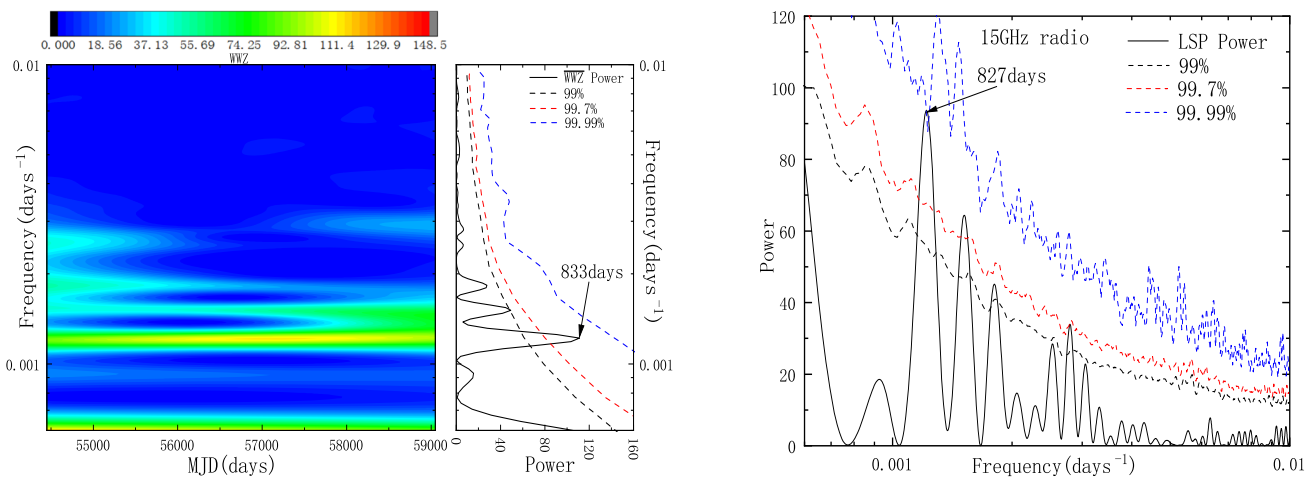
Fig. 5 Same as Fig. 4, but with the 15 GHz radio

**Table 2** Summary of the correlation results between the three bands of 4FGL J0112.1+2245 for all data

Wavebands pair	γ-ray VS. Optical (bin = 30 days)	γ-ray VS. Optical (bin = 7 days)	γ-ray VS. Radio (bin = 30 days)	γ-ray VS. Radio (bin = 7 days)	Radio VS. Optical
$T_{overlap}$[a] (days)	3052	3052	4320	4333	3052
τ_{center} (days)	5 ± 5.6	1 ± 6.4	66 ± 6.9	53 ± 3.5	-73 ± 4.4
DCF peak	0.97 ± 0.05	0.57 ± 0.06	0.35 ± 0.07	0.25 ± 0.03	0.68 ± 0.03
Conf.[b]	>99.7%	> 99.7%	>95%	>95%	>99.7%
Comment[c]	strong	strong	weak	weak	strong

Notes:

[a]The lengths of overlapping time between three bands

[b]The confidence level of correlation coefficient signal

[c]Comment on DCF analysis results
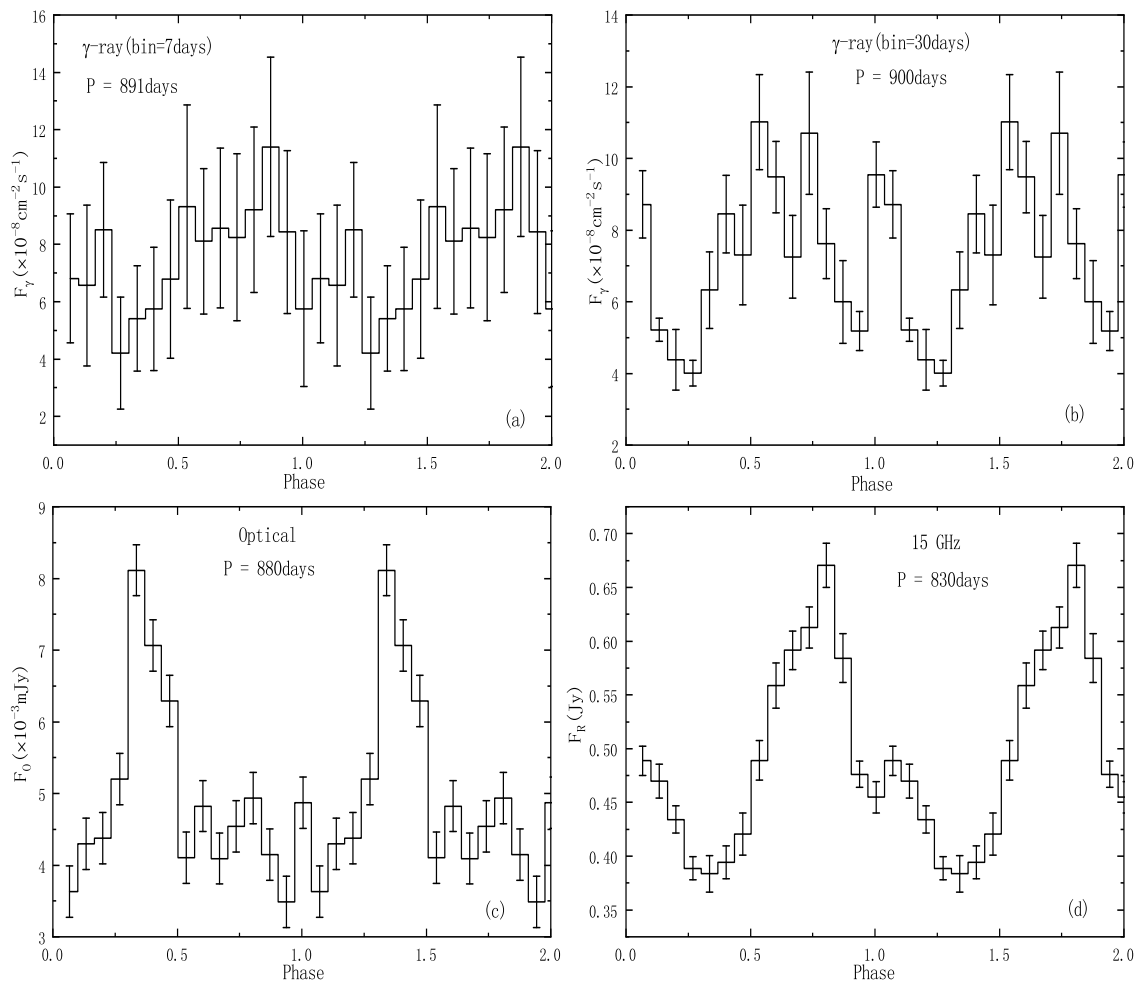
Fig. 6 The epoch-folded pulse shape (two period cycles) results of J0112.1+2245. Panels (**a**), (**b**), (**c**), and (**d**) show the results of the γ-ray (bin = 7 day), γ-ray (bin = 30 day), optical and radio band light curves, respectively

Table 3 The correlation analysis results of light curves ranged from MJD 57670 to 59000

Wavebands pair	γ-ray VS. Optical (bin = 30 days)	γ-ray VS. Optical (bin = 7 days)	γ-ray VS. Radio (bin = 30 days)	γ-ray VS. Radio (bin = 7 days)	Radio VS. Optical
$T_{overlap}$[a] (days)	1277	1277	1515	1515	1277
τ_{center} (days)	-9 ± 7.8	-23 ± 4.7	66 ± 5.3	75 ± 4.1	-94 ± 3.2
DCF	1.15 ± 0.08	0.68 ± 0.05	0.83 ± 0.03	0.64 ± 0.04	0.81 ± 0.04
$Conf.$[b]	>99.7%	>99.7%	>99.7%	>99.7%	>99.7%
$Comment$[c]	strong	strong	strong	strong	strong

Note: The symbols a, b, c are same as Table 2

periodogram, which represents a possible QPO of 827 ± 35 days. The half-width at the half-maximum (HWHM) of the peak was taken as a measure for the uncertainty in the value of QPO.

In order to cross-validate the possible QPO of this source, we further used the Weighted Wavelet Z-transform (WWZ) method for the QPO search. We construct the WWZ spec-

tra using a Morlet mother function for each artificial light curve (Foster 1996; Ackermann et al. 2015; Bhatta 2017, 2019). WWZ analysis can process non-equal interval data, and reduce the influence of astronomical observation signals from the observation season, weather, and moon phases. The phase folding of the point source may provide additional clues to search the QPO of each band. (Agarwal et al. 2021).
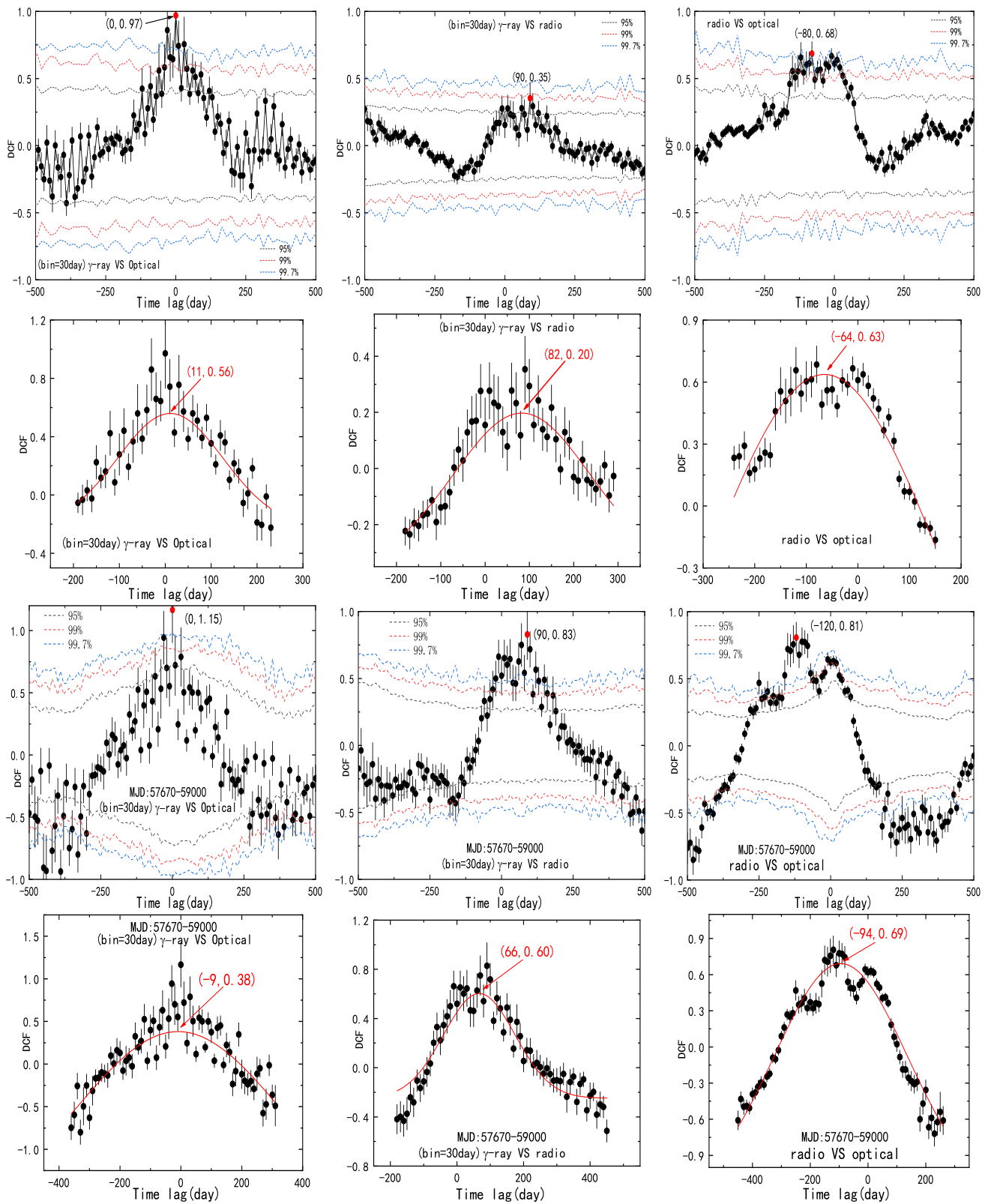
Fig. 7 The first row panels: The Discrete Correlation Function (DCF) analysis results of the Multi-wavelength bands for 4FGL J0112.1+2245. The second row represents the corresponding DCF peaks Gauss fit. The red solid line represent the Gaussian fits. The third row panels: The DCF results of light curves of time interval MJD:57670-59000. The fourth row is the same as the second row, but the MJD range is 57670 to 59000. The black, red, and blue dashed lines represent the confidence level of 95%, 99%, and 99.7% respectively

The results of phase folding are shown in Fig. 6. The error in the period is estimated by calculating the HWHM of the shape of maximum in the time-averaged WWZ power, as shown in the left panel of Figs. 2–5. The detailed results calculated by WWZ are shown in Table 1.

4 The correlation analysis

Discrete correlation function (DCF) is one of the methods used to analyze the correlation between two sets of discrete data (Edelson and Krolik 1988; Hufnagel and Bregman 1992). The biggest feature of this method is that the correlation between two sets of data can be determined without any interpolation processing of the data. The DCF method was introduced by Edelson when studying the time delays of two light curves. The time delay is used to study the structure and other properties of the source (Elvis et al. 1994). For two time series with observations $[a_1, a_2, \ldots a_n]$, $[b_1, b_2, \ldots b_n]$, the DCF is defined through the unbinned discrete correlation:

$$UDCF_{ij} = \frac{(a_i - \bar{a}) \times (b_j - \bar{b})}{\sqrt{(\sigma_a^2 - e_a^2)(\sigma_b^2 - e_b^2)}}, \qquad (6)$$

where $\bar{a}$ and $\bar{b}$ are the average values of the data series a_i and b_i, respectively, σ_a and σ_b are the corresponding standard deviations.

Each value $UDCF_{ij}$ is related to the delay $\triangle t_{ij} = t_j - t_i$. For those noisy data, we can use this formula $[(\sigma_a^2 - e_a^2)(\sigma_b^2 - e_b^2)]^{1/2}$ instead of σ_a^2, σ_b^2 in the above formula. e_a and e_b are the corresponding the average uncertainty. For a given τ, if there are M $UDCF_{ij}$ satisfying $\tau - \triangle \tau/2 \leq \triangle t_{ij} < \tau + \triangle \tau/2$, then average these M data points to get:

$$DCF(\tau) = \frac{1}{M} \sum UDCF_{ij}, \qquad (7)$$

where $DCF(\tau)$ is the discrete correlation function. In the graph of the discrete correlation function, the larger the peak value of DCF, the stronger the correlation between the two series of data, otherwise the opposite. If the peak value of DCF is on the side greater than zero, it means that data a is ahead of data b. If the peak value of DCF is on the side less than zero, it means that data lags behind data b.

The analytical results of DCF are displayed in Fig. 7. We explored time lags ranging from -500 to 500 days. The main central peaks in the resulting of DCFs are fit with a Gaussian function to determine the time lag (τ_{center}) and its uncertainty. To estimate the statistical significance of the DCF peak, we used a power spectral density index with a range of 0.3–1.1 for different wavebands pair. We simulate 2000 light curves with the Monte Carlo method used by Timmer and Koenig (1995). In the simulation, we used the power spectral density index obtained by fitting the spectrum with power law (Yang et al. 2020). Then we evaluate the significance of the correlation between the pair bands (Max-Moerbeck et al. 2014). The black, red, and blue dashed lines in Fig. 7 represent the confidence level of 95%, 99%, and 99.7%, respectively.

From Fig. 7, the whole data analysis can find that there is a significant peak a time lag of $\tau \simeq 5$ days in the γ-ray (30 days bin) versus optical panel, $\tau \simeq 1$ days in the γ-ray (7 days bin) versus optical panel, $\tau \simeq 66$ days in the γ-ray (30 days bin) versus radio panel, $\tau \simeq 53$ days in the γ-ray (7 days bin) versus radio panel, and $\tau \simeq -73$ days in the radio versus optical panel. This suggests that the emission of 15 GHz radio lags behind the optical R band, and it is possible that optical and γ-ray are almost simultaneous (the time delay is close to 0 days). The peaks of the DCF coefficient and confidence levels are shown in Table 2. As shown in Table 2, there is a strong correlation between γ-ray and optical, and between radio and optical, while the correlation between γ-ray and radio is very weak.

5 Discussion and conclusions

Investigating the correlation between different wavebands can promote our understanding of the radiation mechanism of blazar and provide constraints on the underlying emission mechanisms. We analyzed multi-wavelength variability of the TeV BL Lac object 4FGL J0112.1+2245 to see if they show any correlations among them and any indications of QPO in the light curves. The DCF method is widely used to calculate correlation coefficients and time delays of light curves of blazars. Based on the historical light curves data of the radio (15 GHz), optical, and γ-ray bands, we calculated DCF between the different wavebands. As shown in Table 2, the maximum correlation coefficient is greater than 0.97 between γ-ray and optical bands, while the minimum correlation coefficient is about 0.25 between γ-ray and radio bands.

The correlations between the radio and optical bands of 4FGL J0112.1+2245 have been previously studied by Ciprini et al. (2004) and MAGIC team (MAGIC Collaboration et al. 2018), they did not find any correlation peaks above 2σ. We analyzed the correlation between the two bands with the latest updated data and found different results, that the correlation between the two bands is very significant, as shown in Fig. 7. This result may be due to similar variations in different bands during MJD 57670 to 59000. To confirm this reason, we only use the new data from MJD 57670 to 59000 for a separate analysis. The detailed analysis results are as shown in Table 3, and we can see that there is a strong correlation between different bands. The level of confidences for all is $> 3\sigma$. This result probably indicates that a major fraction of the optical flux in this source

is originating from the same emission region as the radio and gamma-ray in the time interval from MJD 57670 to 59000. In the previous time intervals, e.g., MJD 54500 to 55000, and MJD 56200 to 56700, there are probably two "orphan" flares in the radio band. In previous studies, no significant correlation was found between the two bands, which may be caused by this kind of "orphan" flare. The "orphan" flares are discussed in detail by Kusunose and Takahara (2006) and MacDonald et al. (2017). Marscher et al. (2008) revealed that the disturbance moving in the inner jet of blazars produces radio to γ-ray outbursts. The leptonic models predict a strong correlation between synchrotron-produced optical and inverse-Compton scattering (ICS) produced γ-ray emission (Marscher et al. 2008; Zheng and Zhang 2011; Zheng et al. 2013; Zheng and Kang 2013). In this kind of model, compared with the thermal radiation component, the synchrotron component is dominant. The time lag between radio and optical is about -73 days, and the correlation coefficient is larger than 0.68. The time lag between γ-ray and radio are about 66 days, and the correlation coefficient is less than 0.35. This result suggests that gamma-ray emission originated upstream of radio emission along with the jet. Because of the gaps in the γ-ray light curve, it is easy to miss the fast outbursts. This may result in a weak correlation between the γ-ray and radio bands. The time lag between different wavebands could be explained by a disturbance propagating in the jet, in which a moving emission region produces the radio to γ-ray activity, implying that the emission region of γ-ray is closer to the central supermassive black hole than ones of optical and radio emission (Li et al. 2016; Zhang et al. 2017a).

In order to search for the QPO of J0112.1+2245, we collected and processed the long-term observation data of the three bands of this source. We simply averaged the QPO results derived from the two methods (WWZ and LSP) to obtain a possible quasi-period of 896 ± 32 days for γ-ray, 880 ± 54 days for optical, and 830 ± 33 days for radio, respectively. From these results, it can be seen that the QPO of the three bands is relatively close. Moreover, based on the red noise simulation, it is found that the QPO significance of the three bands is above 99.7% ($3\,\sigma$). However, there is another significant QPO (346 days) for the γ-ray band that is about 1 yr, so it may be related to the period of the orbital motion of the Earth. The periodicity of variability can be reasonably explained by the nonballistic helical motion of the emitting material (Li et al. 2016). So far, the QPO theoretical model of blazars has been mentioned by many authors (Ackermann et al. 2015; Zhou et al. 2018).

A kind of QPO theoretical model of blazars is probably related to the orbital timescale of a hot spot, a blob, a flare, or other oscillation phenomena in the innermost portion of the rotating accretion disk (Gupta et al. 2019). For the parameter P involved in the following calculation, we take the

QPO average (889 days) of the three bands. Based on this hypothesis, that the quasi-periodic injection of plasma from an oscillating accretion disk pour into the jet, the formula of SMBH mass is as follows:

$$\frac{M}{M_\odot} = \frac{3.23 \times 10^4 \delta P}{(r^{3/2} + a)(1 + z)}, \tag{8}$$

where P is the value of the observed QPO period in unit of second, δ is Doppler factor, for this cource $\delta = 8.5$, r is radius of this source zone in units of GM/c^2, z is the redshift, a is SMBH spin parameter. Based on the equation (8), we get an SMBH mass estimate of $1.1 \times 10^{12} M_\odot$ for the Schwarzschild limit (with $r = 6.0$ and $a = 0$) and $7.1 \times 10^{12} M_\odot$ for the maximal Kerr limit (with $r = 1.2$ and $a = 0.9982$) (Gupta et al. 2019). In this hypothetical scenario, the estimated black hole mass is too large. Therefore, assuming that QPO comes from perturbations on the innermost stable circular orbit may not be suitable for this Source.

The supermassive binary black hole (SMBBH) model has been successfully applied to explain some of the periodic observational phenomena of blazars (Sillanpaa et al. 1988; Valtonen et al. 2011; Zhang et al. 2017b). This model means that the QPO region has a strong geometric effect. It is assumed that the physical possible reason for QPO is the helical motion of jet, which is periodically disturbed by the secondary black hole in the binary system. The real physical driving period P_d of the helical motion can be estimated by the formula (Rieger 2004):

$$P_d \simeq \frac{\gamma_b^2}{1 + z} P, \tag{9}$$

where z is the redshift, γ_b is the bulk Lorentz factor, and P is the value of the observed QPO period in unit of day. For 4FGL J0112.1+2245, the bulk Lorentz factor is $\gamma_b \sim 7.5$ (Nemmen et al. 2012). If the mass ratio between the primary and secondary black holes less than 3 ($R \leq 3$), we call it "major merger"; if $3 \leq R \leq 10^4$, it is "minor merger" (Kauffmann and Haehnelt 2000; Springel et al. 2005). If the SMBBH mass ratio is known, the mass of the primary black hole can be estimated by the formula (Begelman et al. 1980; Ostorero et al. 2004; Li et al. 2015):

$$M \simeq P_d^{\frac{8}{5}} R^{\frac{3}{5}} M_\odot, \tag{10}$$

where R is the mass ratio and P_d is the value of the QPO in unit of year. For the major merger of the SMBBH system, the mass ratio can be assumed that $R = \frac{3}{2}$. The parameter value is put into the formula to get the mass of the primary black hole is $M \simeq 2.2 \times 10^9 M_\odot$. Other parameters remain unchanged, if $\gamma_b \sim 15$ was adopted, $M \simeq 2.0 \times 10^{10} M_\odot$. For the minor merger of the SMBBH system, assuming $R = 25$, put $\gamma_b \sim 7.5$ and $\gamma_b \sim 15$, according the equation (9), we get the corresponding primary black

hole masses, $M \simeq 1.2 \times 10^{10} M_\odot$ and $M \simeq 1.1 \times 10^{11} M_\odot$, respectively. Comparatively speaking, the black hole mass $M \simeq 2.2 \times 10^9 M_\odot$ based on the helical motion of the jet is more reasonable. The helical motion of the jet is most likely driven by the orbital motion in the SMBBH system, which implies that 4FGL J0112.1+2245 is a possible candidate of SMBBH. Since the observation data lasts only about 10 years and are also affected by some other external factors, the reliability of the QPO in this BL Lac needs further observations to confirm.

References

Abdo, A.A., Ackermann, M., Ajello, M., et al.: Astrophys. J. **32**, 193 (2009)

Abdo, A.A., Ackermann, M., Ajello, M., et al.: Astrophys. J. **715**, 429 (2010)

Ackermann, M., Ajello, M., Albert, A., et al.: Astrophys. J. Lett. **813**, L41 (2015)

Angel, J.R.P., Stockman, H.S.: Annu. Rev. Astron. Astrophys. **18**, 321 (1980)

Ansoldi, S., Antonelli, L.A., et al. (MAGIC Collaboration): Mon. Not. R. Astron. Soc. **480**, 879 (2018)

Atwood, W.B., Abdo, A.A., Ackermann, M., et al.: Astrophys. J. **697**, 1071 (2009)

Aleksić, J., Ansoldi, S., Antonelli, L.A., et al.: Astron. Astrophys. **576**, A126 (2015)

Agarwal, A., Rani, P., Prince, R., et al.: Galaxies **9**, 20 (2021)

Begelman, M.C., Blandford, R.D., Rees, M.J.: Natur **287**, 307 (1980)

Bessell, M.S.: Publ. Astron. Soc. Pac. **91**, 589 (1979)

Bhatta, G.: Astrophys. J. **847**, 7 (2017)

Bhatta, G.: Mon. Not. R. Astron. Soc. **487**, 3990 (2019)

Cavaliere, A., Padovani, P.: Astrophys. J. Lett. **340**, L5 (1989)

Chokshi, A., Turner, E.L.: Mon. Not. R. Astron. Soc. **259**, 421 (1992)

Ciprini, S., Tosti, G., Teräsranta, H., Aller, H.D.: Mon. Not. R. Astron. Soc. **348**, 1379 (2004)

Charisi, M., Bartos, I., Haiman, Z., et al.: Mon. Not. R. Astron. Soc. **463**, 2145 (2016)

Dai, B.Z., Zhang, B.K., Zhang, L.: New Astron. **11**, 471 (2006)

Edelson, R.A., Krolik, J.H.: Astrophys. J. **333**, 646 (1988)

Elvis, M., Wilkes, B.J., McDowell, J.C., et al.: Astrophys. J. Suppl. Ser. **95**, 1 (1994)

Foster, G.: Astron. J. **112**, 1709 (1996)

Gaur, H., Gupta, A.C., Wiita, P.J.: Astron. J. **143**, 23 (2012)

Graham, M.J., Djorgovski, S.G., Stern, D., et al.: Mon. Not. R. Astron. Soc. **453**, 1562 (2015a)

Graham, M.J., Djorgovski, S.G., Stern, D., et al.: Nature **518**, 74 (2015b)

Gupta, A.C., Tripathi, A., Wiita, P.J., et al.: Mon. Not. R. Astron. Soc. **484**, 5785 (2019)

Hufnagel, B.R., Bregman, J.N.: Astrophys. J. **386**, 473 (1992)

Kauffmann, G., Haehnelt, M.: Mon. Not. R. Astron. Soc. **311**, 576 (2000)

Kusunose, M., Takahara, F.: Astrophys. J. **651**, 113 (2006)

Li, H.Z., Chen, L.E., Yi, T.F., et al.: Publ. Astron. Soc. Pac. **127**, 1 (2015)

Li, H.Z., Jiang, Y.G., Guo, D.F., et al.: Publ. Astron. Soc. Pac. **128**, 074101 (2016)

Li, X.P., Luo, Y.H., Yang, H.Y., et al.: Astrophys. Space Sci. **363**, 169 (2018)

Lomb, N.R.: Astrophys. Space Sci. **39**, 447 (1976)

Mattox, J.R., Bertsch, D.L., Chiang, J., et al.: Astrophys. J. **461**, 396 (1996)

Marscher, A.P., Jorstad, S.G., D'Arcangelo, F.D., et al.: Nature **452**, 966 (2008)

Max-Moerbeck, W., Hovatta, T., Richards, J.L., et al.: Mon. Not. R. Astron. Soc. **445**, 428 (2014)

MacDonald, N.R., Jorstad, S.G., Marscher, A.P.: Astrophys. J. **850**, 87 (2017)

Nemmen, R.S., Georganopoulos, M., Guiriec, S., et al.: Science **338**, 1445 (2012)

Ostorero, L., Villata, M., Raiteri, C.M.: Astron. Astrophys. **419**, 913 (2004)

Press, W.H., Teukolsky, S.A., Vetterling, W.T., Flannery, B.P.: nrfa.book (1992)

Peñil, P., Domínguez, A., Buson, S., et al.: Astrophys. J. **896**, 134 (2020)

Richards, J.L., Max-Moerbeck, W., Pavlidou, V., et al.: Astrophys. J. Suppl. Ser. **194**, 29 (2011)

Rieger, F.M.: Astrophys. J. Lett. **615**, L5 (2004)

Robson, E.I., Litchfield, S.J., Gear, W.K., et al.: Mon. Not. R. Astron. Soc. **262**, 249 (1993)

Ren, G.W., Zhang, H.J., Zhang, X., et al.: Res. Astron. Astrophys. **21**, 075 (2021)

Scargle, J.D.: Astrophys. J. **263**, 835 (1982)

Sillanpaa, A., Haarala, S., Valtonen, M.J., et al.: Astrophys. J. **325**, 628 (1988)

Springel, V., White, S.D.M., Jenkins, A., et al.: Nature **435**, 629 (2005)

Shaw, M.S., Romani, R.W., Cotter, G., et al.: Astrophys. J. **764**, 135 (2013)

Sobacchi, E., Sormani, M.C., Stamerra, A.: Mon. Not. R. Astron. Soc. **465**, 161 (2017)

Timmer, J., Koenig, M.: Astron. Astrophys. **300**, 707 (1995)

Urry, C.M., Padovani, P.: Publ. Astron. Soc. Pac. **107**, 803 (1995)

Valtaoja, L., Takalo, L.O., Sillanpaa, A., et al..: Astron. J. **102**, 1946 (1991)

Valtaoja, L., Sillanpaa, A., Valtaoja, E.: Astron. Astrophys. **184**, 57 (1987)

Vaughan, S., Edelson, R., Warwick, R.S., et al.: Mon. Not. R. Astron. Soc. **345**, 1271 (2003)

Valtonen, M.J., Lehto, H.J., Takalo, L.O., Sillanpää, A.: Astrophys. J. **729**, 33 (2011)

Wu, Z., Jiang, D.R., Gu, M., Liu, Y.: Astron. Astrophys. **466**, 63 (2007)

Wu, Z.Z., Gu, M.F., Jiang, D.R.: Res. Astron. Astrophys. **9**, 168 (2009)

Xiong, D., Bai, J., Zhang, H., et al.: Astrophys. J. Suppl. Ser. **229**, 21 (2017)

Yan, D., Zhou, J., Zhang, P., et al.: Astrophys. J. **867**, 53 (2018)

Yang, X., Yi, T.F., Zhang, Y., et al.: Publ. Astron. Soc. Pac. **132**, 044101 (2020)

Zheng, Y.G., Zhang, L.: Astrophys. J. **728**, 105 (2011)

Zheng, Y.G., Zhang, L., Huang, B.R., Kang, S.J.: Mon. Not. R. Astron. Soc. **431**, 2356 (2013)

Zheng, Y.G., Kang, T.: Astrophys. J. **764**, 113 (2013)

Zhang, B.K., Zhao, X.Y., Zhang, L., Dai, B.Z.: Astrophys. J. Suppl. Ser. **231**, 14 (2017a)

Zhang, P.F., Yan, D.H., Liao, N.H., et al.: Astrophys. J. **835**, 260 (2017b)

Zhou, J., Wang, Z., Chen, L., et al.: Nat. Commun. **9**, 4599 (2018)

Zhang, P.F., Yan, D.H., Zhou, J.N., et al.: Astrophys. J. **891**, 163 (2020)